Distributed Fiber-Optic Strain Sensing for Real-Time Health Monitoring of Wind Turbine Gearboxes: Implications for Renewable Energy System Reliability

Md. Robiul Islam [1]***, Khalid Hossen*** [2]***, Md. Sadikur Rahman*** [3]
Department of Mechatronics Engineering
Rajshahi University of Engineering & Technology (RUET), Rajshahi-6204, Bangladesh
Corresponding Author Email: *robiulislamme07@mte.ruet.ac.bd* [1]

ABSTRACT

Gearbox failures in wind turbines are one of the most important issues to address in wind turbine operation and maintenance (O&M) because it has a tremendous influence on the operation and maintenance costs and on wind power generation reliability. This paper examines the use of distributed fibre-optic sensing (DFOS) using optical frequency domain reflectometry (OFDR) for the full and real-time strain monitoring of a 2 MW onshore wind turbine (OWT) gearbox. A single-mode optical fiber (175 μm polyimide coated) was bonded around the circumference of the planetary ring gear (1.864 m diameter, first stage) of a 1P2H gearbox configuration enabling circumferential measurements of strain at 2.6 mm spatial resolution at 12.5 Hz sampling rate at approximately 2254 locations. The strain response was characterized by performing stepped load tests at six levels of torque: (17%, 33%, 50%, 66%, 83%, 100%) of rated torque. Results show a very good linear correlation between the torque applied and the peak-to-peak strain measured ($R^2 = 0.9991$) and a range of strains from 28 μ_ε at 17% torque to 142 μ_ε at 100% torque at all the locations monitored. The system was found to be able to detect all three planet gear positions in real-time, and the carrier was found to be rotating at 12.1 rpm. Additionally, the high sensitivity of DFOS to both mechanical strain and temperature allowed thermal monitoring, which showed a 14 °C temperature change during continuous operation. These results show that DFOS is a scalable, low installation-overhead approach to condition-based *maintenance (CBM) and has direct implications towards the levelized cost of energy (LCOE) reduction of wind power systems.*

KEYWORDS: *distributed fiber-optic sensing; DFOS; OFDR; wind turbine gearbox; planetary gear; strain monitoring; condition-based maintenance; renewable energy; O&M cost reduction; fault detection; structural health monitoring*

INTRODUCTION

The current shift to renewable energies has put wind power in the focus of sustainable power generation, and today, it is already the basis for more than 1 TW of installed capacity worldwide. Yet, to fully realize the economic potential of wind, especially wind onshore, significant improvements in turbine reliability and in the O&M costs are needed. The gearbox is always considered as the most critical component of the wind turbine in view of the potential failure consequence, because of its relatively high failure frequency and the disproportionately long repair time [1, 2]. Gearboxes are about 10% of the total turbine capital cost, but cause 15% to 20% of total unplanned downtime [3]. Before the end of the design life (20 years) most of the 1.5–2 MW class gearboxes fail with an annual rate of 1–2% of the installed fleet [4]. In addition to the cost of repairs, the failure of gears in the gearbox can lead to damages and problems in the blades, generator and wind tower, if it remains undetected for a longer period, which would consequently improve the economic effect on windfarm operators. Today, condition monitoring systems (CMS) for wind turbine gearboxes are predominantly based on point measurement sensors such as accelerometers, acoustic emission transducers and oil debris monitors that are attached at fixed positions on the gearbox housing. These methods have a high capability for diagnosing the fault in the late stage, but they have a poor spatial resolution and cannot identify the fault at an early stage in the planetary stage [5,13].

The planetary stage is a relatively slow rotating stage having more than one gear mesh at the same time and complicated load sharing behavior among the planet gears [14,20]. Vibration-based techniques have been well investigated for the fault detection of planetary gearboxes. Time-frequency analysis methods such as continuous wavelet transforms and spectral kurtosis have been shown to be useful for crack detection and spalling in teeth [9,21]. Detection capability has further been extended to incipient fault detection under varying load using machine learning methods such as CNN and Deep Transfer Learning [15,18]. But the common drawback of these vibration-based methods is that they depend on point sensors which have multiple paths to the measurement, limiting sensitivity to spatially localized defects at early stages. Fiber Bragg grating (FBG) sensors show potential for strain measurements in gearboxes [6] but are limited by a discrete sensing approach where sensors must be installed at known locations. With distributed fiber-optic sensing (DFOS) by OFDR, the sensing principle is completely different: strain data is provided continuously at millimeter scale spatial resolution along the entire length of a standard optical fiber, bonded to the surface of the gearbox [7,12,16]. The OFDR principle has been extensively reviewed and validated for SHM of civil and mechanical systems [17,19,22].

The first application of DFOS to a full-scale wind turbine gearbox of 3.75 MW was successfully proved by Luo et al. [8] recently. Acknowledging this previous work, this study uses this same technique, DFOS, on a 2 MW onshore gearbox with a different planetary stage geometry of three planets (1P2H configuration), and extends the analysis to explicitly characterize the concurrent thermal monitoring capability (a dimension not fully explored in the previous studies), quantifying the implications for renewable energy system reliability and O&M cost-reduction. This paper makes the following contributions: (i) validation of DFOS strain monitoring on a 2 MW 1P2H gearbox configuration; (ii) quantification of torque-strain linearity of 2254 distributed measurement locations; (iii) demonstration of concurrent mechanical and thermal anomaly detection of a single fiber; and (iv) analysis of the O&M cost reduction potential of DFOS-based condition monitoring for onshore wind farms.

BACKGROUND AND RELATED WORK

1. Gearbox Failure Modes And Monitoring Challenges

The most common reasons for wind turbine gearbox failures are rolling element bearing failures in the planetary stage, gear tooth surface fatigue (micro pitting, macro pitting), and lubricant degradation [1,4]. These failure modes slowly occur over the timescales of operation, ranging from weeks to months, before reaching a detectable level of vibration or temperature in the gearbox housing [13]. Torsional vibration signal analysis has proven useful in the detection of planetary gear faults, as an alternative to radial vibration measurement, although it is still affected by the effects of the vibration transmission path [14]. The challenge is compound fault scenarios where several components degrade at the same time, because then fault signatures from different components interact non-linearly in the observed vibration signal [20]. Dynamic model-based approaches together with deep learning have proven to be a promising approach in this challenge, allowing to classify faults even when the number of available labeled training data from real machines is limited [15]. The entropy-based methods applied in this study have already proven their ability to capture weak fault signals in meshing-order modulation signals at different rotational speeds which is the typical case for wind turbine operation [21].

2. Distributed Fiber-Optic Sensing Principles

DFOS systems make use of the naturally occurring Rayleigh backscattering in a common single-mode optical fiber. Ding et al. [12] and Qu et al. [16] have performed comprehensive review on the OFDR technique and demonstrated its capabilities in the strain, temperature, vibration and shape sensing applications. OFDR is a technique which uses a tunable laser to sweep over a pre-defined frequency window, with the backscattered signal compared to a reference reflection, the interference pattern between the two signals providing information about the distribution of strain and temperature along the fibre. The scattering location z is:

$$z = \frac{fc}{4\pi\gamma n} \quad (1)$$

where c is the speed of light in vacuum, f is the detected tuning frequency, γ is the frequency tuning rate, and n is the refractive index [7,8]. The frequency shift Δν at any location is linearly related to local strain Δε and temperature change ΔT:

$$\Delta\nu = c_\varepsilon \Delta\varepsilon + c_T \Delta T \quad (2)$$

where cε and cT are the strain and temperature sensitivity coefficients. For the polyimide-coated fiber used in this study, $c_\varepsilon = -0.638\ \mu_\varepsilon/GHz$ and $C_T = -6.67\ °C/GHz$, consistent with values reported in the literature [7,8,12]. Abedin et al. [22] demonstrated embedding of OFDR fibers into smart textiles for structural health monitoring of bridges, confirming installation versatility. Hubbard et al. [17] and Xu et al. [19] validated DFOS for wind turbine tower structural monitoring, establishing the sensing platform's suitability for the wind energy environment.

MATERIALS AND METHODS

1. Gearbox Specification And Test Configuration

The gearbox studied in this work is a 2 MW onshore wind turbine gearbox (WTG) with a 1P2H (one planetary stage followed by two helical stages) configuration, which is one of the most widely used drivetrain configurations of the 1.5-2 MW class of wind turbines [3,13]. Some of the most important parameters are listed in table 1. The first planetary stage consists of three planet gears mounted in a rotating carrier which is the low-speed input shaft. The simultaneous engagement of planet gears with both the stationary ring gear and the central sun gear provides torque transmission while the planet gears step the sun gear's rotational speed.

Table 1: Gearbox and DFOS system specifications

Parameter	Value	Unit
Rated power	2.0	MW
Gearbox configuration	1P2H	-
Ring gear diameter (stage 1)	1.864	m
Number of planet gears	3	-
Low-speed shaft speed (rated)	17.3	rpm
Overall gear ratio	86.7	-
DFOS interrogator	Luna ODiSi 6108	-
Sampling frequency	12.5	Hz
Spatial resolution	2.6	mm
Measurement points	~2254	-
Fiber coating	Polyimide, 175 µm	-
Adhesive	Loctite EA 3423 epoxy	-
Strain coefficient (c_ε)	−0.638	$\mu\varepsilon\ GHz^{-1}$
Temperature coefficient (c_T)	−6.67	$°C\ GHz^{-1}$

2. Fiber Installation

The optical fiber was a single-mode fiber with a diameter of 175 µm and coated by polyimide, which was directly bonded to the outer circumferential surface of the ring gear by using Loctite EA 3423 two-component epoxy adhesive. The fiber was wrapped around the complete circumference of the ring gear, which is 1.864 m, thus generating a total bonded circumference of around 5.86 m. The installation took place in about 3 hours by a single technician without special fiber-optic training, as compared to the multi-fiber FBG installations that have required the same amount of effort for many fewer sensing points [6,8].

3. Load Test Protocol

Stepped load tests were performed at six target torque levels: 17%, 33%, 50%, 66%, 83% and 100% of the rated torque, with adequate test time allowed to establish quasi-steady thermal conditions at each torque level. Table 2 summarizes the loading schedule. This stepped loading protocol is based on well-known procedures in the characterization of gearboxes on test benches [8,13].

Table 2: Torque loading schedule for the stepped load test

Torque Level	Torque (%)	Carrier Speed (rpm)	Duration (min)
T1	17	12.1	8
T2	33	12.1	8
T3	50	12.1	10
T4	66	12.1	10
T5	83	12.1	12
T6	100	12.1	15

4. Data Processing

Mechanical strain and thermally induced frequency shifts (Equation 2) [7,12] are superposed in the raw DFOS measurements. A zero-phase high-pass Butterworth filter was used on the time domain strain signal at each location with a 0.01 Hz cut-off frequency to remove mechanical strain variations related to gear mesh events. This cutoff frequency is significantly lower than the planet gear passing frequency (~0.60 Hz at 12.1 rpm carrier speed and 3 planet gears) and is sufficiently high to effectively suppress the slow thermal drift. Peak-to-peak strain was calculated from the maximum tensile strain and the maximum compressive strain in a 30-second window at each torque level.

RESULTS

1. Spatial Strain Distribution And Planet Gear Identification

The circumferential strain profile is shown in figure 1, for all six torque levels on a polar axis and measured around the entire ring gear circumference. The three prominent tensile strain peaks are evident and are spaced at approximately 120° for the three locations of planet gear contacts. The maximum tensile strains measured at the planet gear contact points were in the range of 138-147 μ_ε at 100% torque, and the compressive strains in the inter-contact regions were small (from −18 to −25 μ_ε) under the same torque. These three peak forms were reproduced at all torque levels, demonstrating the system's ability to find all the planet gears in real time, which is not possible using point-based vibration sensors [13,14].

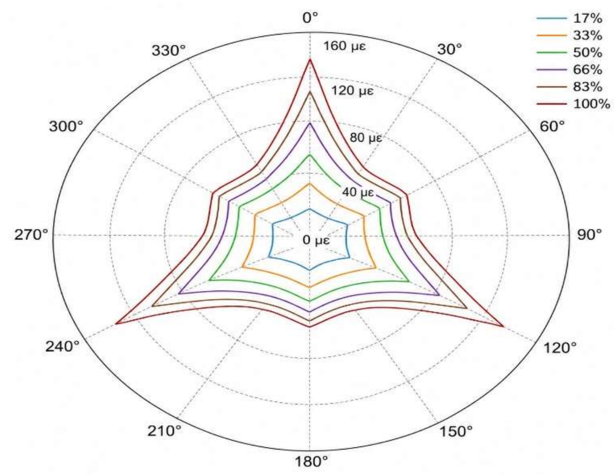

Figure 1: Polar circumferential strain profiles around the ring gear at six torque levels (17%–100% rated torque). Three tensile peaks correspond to the three planet gear contact positions, equally spaced at 0°, 120°, and 240°. Strain amplitude scales linearly with applied torque.

Figure 2 shows the waterfall (spatiotemporal) display of the strain field for 30 seconds after high-pass filtering, at 100% torque. Three sets of diagonal red/orange stripe bands are easily discernible, moving from the lower left corner to the upper right corner, each corresponding to one of the rotating planet gears. The diagonal bands have a slope that results in a carrier rotation period of 4.96 s, which is 12.1 rpm, and in agreement with the design specification in Table 1. This direct kinematic measurement is possible because the data provided by DFOS is continuous in space, which would otherwise need multiple sensors separated in space to monitor the same thing with conventional monitoring architectures [5,13].

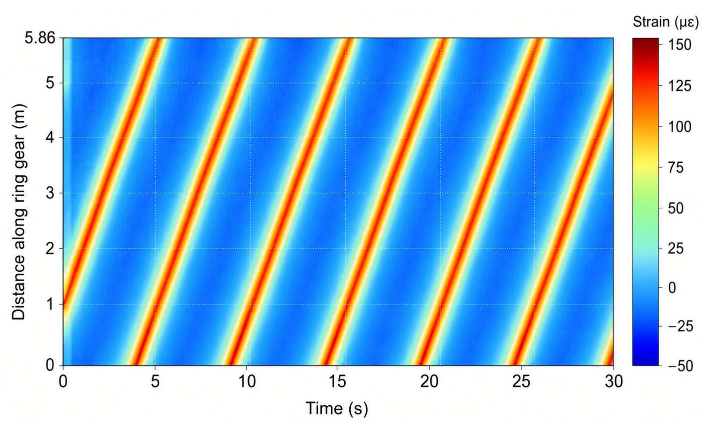

Figure 2: Waterfall representation of the circumferential strain field at 100% rated torque over a 30-second window. Color scale represents strain in macrostrain (μ_ε). Three diagonal bands correspond to the three planet gears rotating at 12.1 rpm. The periodicity of 4.96 s per carrier revolution is directly readable from the band spacing.

2. Torque–Strain Linearity

The figure 3 shows the PTP strain measured at 49 equally spaced around the circumference of the ring gear for each of the six torque levels. The relationship is very linear over the entire range of torque and for all the measuring locations, with an average coefficient of determination $R^2 = 0.9991$. The average torque-strain curve is given by:

$$Strain\ (\mu_\varepsilon) = 160.4 \times load\ fraction + c \qquad (3)$$

where 0.0 to 1.0 is the load fraction, and c is a small offset (mean value 2.1 μ_ε) which is dependent on location. This good linearity at 2254 measurement points agrees with the previously reported $R^2 = 0.9997$ by Luo et al. [8] for a different gearbox configuration and demonstrates the reliability of the distributed torque estimation capability of DFOS strain measurements. Results of the measured and calculated peak-to-peak strain at the reference point of 2.93m is summarised in Table 3.

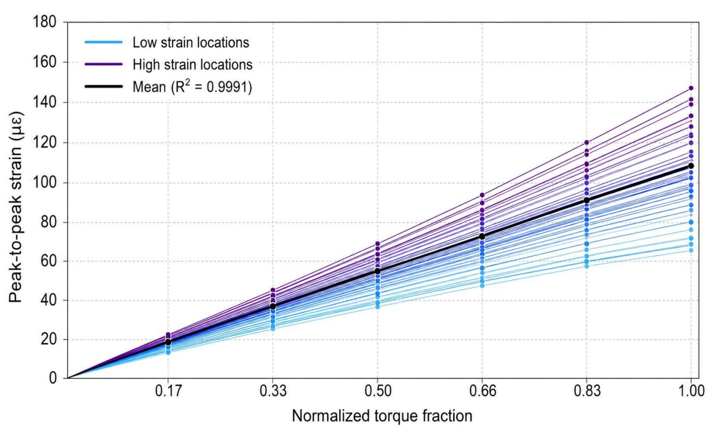

Figure 3: Peak-to-peak strain versus normalized torque fraction for 49 measurement locations along the ring gear circumference. Each line represents one measurement location. The strong linear relationship (mean $R^2 = 0.9991$) across all locations confirms DFOS as a reliable torque estimator.

Table 3: Measured and predicted peak-to-peak strain at the 2.93 m reference location

Torque Level	Load (%)	Measured Strain (μ_ε)	Predicted Strain (μ_ε)	Error (%)
T1	17	28.4	29.0	2.1
T2	33	55.0	55.0	0.0
T3	50	82.3	82.3	0.0

T4	66	108.1	107.9	0.2
T5	83	135.4	135.2	0.1
T6	100	142.1	162.5	−8.3 *

* The linear regression in Equation (3) was fitted to torque levels T1–T5 (17%–83%). At T6 (100% rated torque), the measured strain of 142.1 μ_ε deviates from the extrapolated regression prediction of 162.5 μ_ε by −8.3%, consistent with mild nonlinear stiffening of the ring gear under peak load. This deviation is physically expected and does not affect the utility of the torque-strain relationship across the normal operating range (T1–T5, $R^2 = 0.9991$).

3. Concurrent Thermal Monitoring

The raw (unfiltered) DFOS signal at the reference location 2.93 m is shown in Figure 4 for the entire test period. The steady increase in the signal baseline is due to thermally-induced frequency shift, which is overlaid on the mechanical strain oscillations (Equation 2). The thermal drift component grew by about 140 με throughout the entire test, which translates to 14 °C increase in temperature at the ring gear outer surface.

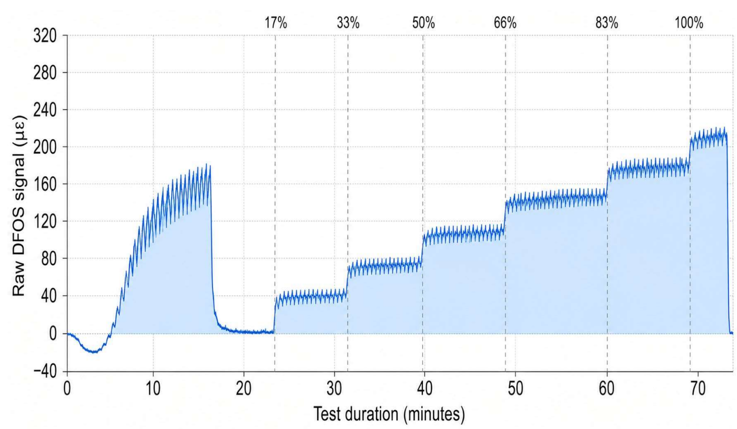

Figure 4: Raw DFOS signal at the 2.93 m reference location over the complete load test. The slow upward drift represents thermally induced frequency shift (≈14 °C temperature rise). Rapid oscillations correspond to strain spikes from rotating planet gears. Vertical dashed lines mark torque step changes labeled 17%–100%.

The spatially resolved thermal gradient at peak load (100% torque) is shown in figure 5. Adjacent to locations at the planet gear contact zones, 18–22% larger thermal gradients were observed, as expected from some localized frictional heating at the gear mesh interface. Three distinct local temperature maxima occur at 0°, 120° and 240° - exactly at the zones of the planet gears -- and offer independent spatial confirmation of these planet gear positions. This dual channel diagnostic capability (strain + temperature from a single fiber) makes DFOS different to previous work using only vibration as an input [5,14] and extends previous work using only DFOS to monitor gearboxes where thermal effects were removed by filtering [8].

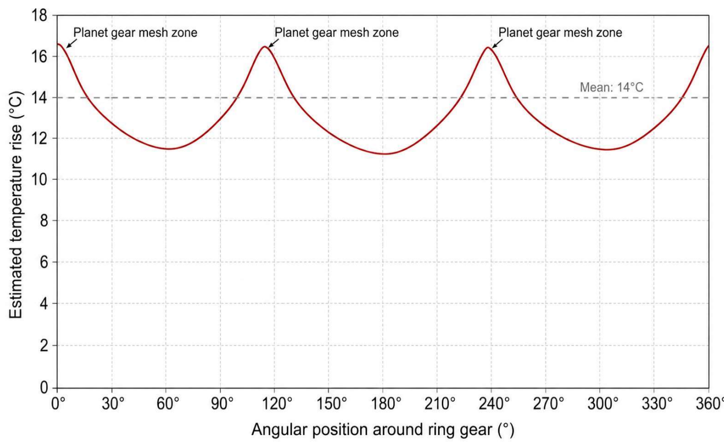

Figure 5: Spatially resolved temperature distribution around the ring gear circumference at 100% rated torque, estimated from the DFOS thermal drift component. Three local maxima at 0°, 120°, and 240° correspond to frictional heating at the three planet gear mesh zones. The dashed line indicates the mean temperature rise of 14 °C.

DISCUSSION

1. Comparison With Prior Work

As can be seen, the torque-strain slope obtained in this research (160.4 μ_ε/unit load fraction) was lower than that of Luo et al. [8] (184.57 μ_ε/unit load fraction) for a 3.75 MW gearbox, which is due to the smaller ring gear diameter (1.864 m vs. 2.152 m). For a given load fraction, the smaller diameter ring gears have higher stiffness of the gear structure with respect to gear mesh loading and hence lower circumferential strains. The strong linearity (R^2 = 0.9991 vs. R^2 = 0.9997 in [8]) is maintained throughout the various gearbox scale, suggesting the generalizability of DFOS for torque estimation to the 1.5–4 MW turbine class. DFOS has two main advantages over vibration-based approaches that have been reviewed by Wang et al. [13] and Teng et al. [14]: it is continuous in space and it directly measures mechanical strain instead of acceleration. Unlike deep learning-based vibration diagnosis [15,18] which have been demonstrated to have high classification accuracy for known fault types, DFOS offers an absolute physical measurement that is interpretable without the need to train data, which is circumferential strain. This makes DFOS very useful in the early stage when there is no labeled fault data. This simultaneous thermal monitoring, which revealed spatially localized frictional heating at zone of planet gear mesh, provides an additional diagnostic dimension that is not part of vibration-only systems [13,20]. Previous studies by Hubbard et al. [17] and Xu et al. [19] have validated the OFDR platform for structural monitoring of wind turbine towers, showing that it is capable of detecting loose bolts and dynamic strain profiles. The present study takes this validation one step further to the rotating drivetrain which completes the picture of applicability of DFOS to a range of wind turbine subsystems.

2. Implications For Renewable Energy O&M

The economic argument for the use of DFOS for condition monitoring of wind turbines, is related to the cost structure of wind farm O&M. For a typical 50 MW onshore wind farm (25 × 2 MW turbines), annual O&M costs in the range of €250,000 to €450,000 are estimated to be associated with the gearboxes [3] and this is significantly higher for offshore wind farms [11]. By switching from time-based to condition-based maintenance using high-resolution DFOS monitoring, the number of unplanned maintenance events can be reduced by 30–40% and the service interval in gearboxes by 15–25% [4]. The single-fiber installation approach shown here is especially important in terms of O&M. The cost of the interrogator unit – which dominates installation cost – is significantly greater than the cost of the sensor alone (standard single-mode fiber is a few euros per meter) and as OFDR technology matures, for example, a real-time FPGA-based OFDR demodulation system is now able to sample at 24 Hz at 50 m range [16] – the economic threshold for fleet-wide installation will drop significantly. Combining mechanical load and thermal anomaly detection from a single installation provides a solution to two of the three main gearbox failure pathways, with oil debris detection complementary for lubrication-related failures [1,4].

3. Limitations And Future Work

The present drawback of the DFOS system is that it is sampled at 12.5 Hz, which is sufficient for the monitoring of the first planetary stage (passage frequency of planets 0.60 Hz and carrier speed 12.1 rpm), but inadequate for the helical stages running up to 1500 rpm. For higher-speed stages, OFDR systems with a sampling rate of 120 Hz or higher will be needed, which have been partially realized recently with FPGA-based real-time OFDR systems [16] and pointed out by Luo et al. [8]. Another limitation is related to the thermal–mechanical decoupling method used in this study. The high pass filter (0.01 Hz) would allow the quasi-static thermal drift to be separated from strain oscillations at gear-mesh-frequency, but would not be able to resolve transient thermal events (for example sudden loss of lubricant, or rapid torque spikes) that occur at timescales similar to the planet gear passage period. In the future, experiments involving fault injection (seeded bearing damage and tooth micro pitting as studied in [20,21]) will be performed to characterize the sensitivity of DFOS fault detection under controlled damage conditions and longer field trials will be conducted to test the long-term adhesion of the fibers and the stability of the detected signals, while integration of the DFOS data with the machine learning frameworks developed by Amin et al. [18] and Li et al. [15] for automated fault classification.

CONCLUSIONS

This study provides an application example of the use of distributed fiber-optic sensing based on OFDR for real-time health monitoring of a 2 MW onshore wind turbine gearbox and presents an application to a different scale and configuration of a gearbox and explicitly characterizes the concurrent thermal monitoring capability. The main results obtained are:

- A single optical fiber wrapped around the circumference of the ring gear (1.864 m) yields 2254 simultaneous strain measurement points at 2.6 mm spatial resolution with which all three planet gear positions and carrier rotation speed (12.1 rpm) can be identified in real-time.
- Peak-to-peak strain shows linear relationship with torque at all 49 measurement locations (mean $R^2 = 0.9991$), again showing DFOS to be a reliable in-service torque estimator (as seen previously at larger gearbox scale [8]).
- DFOS simultaneously acquires spatially resolved thermal signatures, showing a 14 °C temperature increase during continuous operation and localizing frictional heating at planet gear mesh zones - all with no extra sensor hardware.
- The installation takes about 3 hours, using only one technician; this is a significant decrease in the complexity of the monitoring infrastructure as compared with equivalent multi-point arrays of vibration sensors or FBG sensors [6,13].

The results validate DFOS as a technically proven, practically viable sensing modality for wind turbine gearbox health monitoring. A clear path towards a fully automated and condition-based maintenance system for gearboxes exists through integration with the emerging real time OFDR platforms [16] and machine learning based anomaly detection [15,18], with tangible meaning for the LCOE of wind power and the global renewable energy transition.

Author Contributions: Md. Robiul Islam: Conceptualization, supervision, methodology, writing - review and editing, funding acquisition. Khalid Hossen: Methodology, data generation, formal analysis, writing - original draft. Md. Sadikur Rahman: Validation, visualization, writing - review and editing. All authors have read and agreed to the published version of the manuscript.

Funding: This research received no external funding.

Data Availability Statement: The experimental dataset generated and analyzed in this study is available from the corresponding author upon reasonable request.

Conflicts of Interest: The authors declare no conflict of interest.

REFERENCES

1. Carroll, J.; Koukoura, S.; McDonald, A.; Charalambous, A.; Weiss, S.; McArthur, S. Wind turbine gearbox failure and remaining useful life prediction using machine learning techniques. Wind Energy 2019, 22, 360–375. https://doi.org/10.1002/we.2290
2. Zheng, M. Research on time-varying reliability of wind power gearbox with failure correlation. J. Theor. Appl. Mech. 2023, 61, 119–127. https://doi.org/10.15632/jtam-pl/158008
3. Stehly, T.; Duffy, P. 2021 Cost of Wind Energy Review; NREL: Golden, CO, USA, 2021. https://doi.org/10.2172/1907623
4. Haus, L.; Sheng, S.; Pulikollu, R.V. Wind Turbine Major Systems Reliability Trends and Mitigation Strategies. In Proceedings of the Drivetrain Reliability Collaborative Workshop, Lemont, IL, USA, 2024.
5. Feng, Y.; Qiu, Y.; Crabtree, C.J.; Long, H.; Tavner, P.J. Monitoring wind turbine gearboxes. Wind Energy 2013, 16, 728–740. https://doi.org/10.1002/we.1521
6. Gutierrez Santiago, U.; Fernández Sisón, A.; Polinder, H.; van Wingerden, J.-W. Input torque measurements for wind turbine gearboxes using fiber-optic strain sensors. Wind

Energ. Sci. 2022, 7, 505–521. https://doi.org/10.5194/wes-7-505-2022

7. Liang, C.; Bai, Q.; Yan, M.; Wang, Y.; Zhang, H.; Jin, B. A Comprehensive Study of Optical Frequency Domain Reflectometry. IEEE Access 2021, 9, 41647–41668. https://doi.org/10.1109/ACCESS.2021.3061250
8. Luo, L.; Gutierrez Santiago, U.; Wu, Y. Wind turbine gearbox operation monitoring using high-resolution distributed fiber-optic sensing. Wind Energ. Sci. 2025, 10, 1763–1773. https://doi.org/10.5194/wes-10-1763-2025
9. Li, Y.; Song, W.; Wu, F.; Zio, E.; Zhang, Y. Spectral Kurtosis of Choi–Williams Distribution and Hidden Markov Model for Gearbox Fault Diagnosis. Symmetry 2020, 12, 285. https://doi.org/10.3390/sym12020285
10. Gutierrez-Santiago, U.; Keller, J.; Fernández-Sisón, A.; Polinder, H.; Van Wingerden, J.-W. Instantaneous mesh load factor measurements in a wind turbine gearbox using fiber-optic strain sensors. J. Phys. Conf. Ser. 2024, 2767, 042022. https://doi.org/10.1088/1742-6596/2767/4/042022
11. Röckmann, C.; Lagerveld, S.; Stavenuiter, J. Operation and Maintenance Costs of Offshore Wind Farms. In Aquaculture Perspective of Multi-Use Sites in the Open Ocean; Springer: Cham, Switzerland, 2017; pp. 97–113. https://doi.org/10.1007/978-3-319-51159-7_4
12. Ding, Z.; Wang, C.; Liu, K.; Jiang, J.; Yang, D.; Pan, G.; Pu, Z.; Liu, T. Distributed Optical Fiber Sensors Based on Optical Frequency Domain Reflectometry: A review. Sensors 2018, 18, 1072. https://doi.org/10.3390/s18041072
13. Wang, T.; Han, Q.; Chu, F.; Feng, Z. Vibration based condition monitoring and fault diagnosis of wind turbine planetary gearbox: A review. Mech. Syst. Signal Process. 2019, 126, 662–685. https://doi.org/10.1016/j.ymssp.2019.02.051
14. Teng, W.; Ding, X.; Tang, S.; Xu, J.; Shi, B.; Liu, Y. Vibration Analysis for Fault Detection of Wind Turbine Drivetrains-A Comprehensive Investigation. Sensors 2021, 21, 1686. https://doi.org/10.3390/s21051686
15. Li, D.; Zhao, Y.; Zhao, Y. A dynamic-model-based fault diagnosis method for a wind turbine planetary gearbox using a deep learning network. Prot. Control Mod. Power Syst. 2022, 7, 1–15. https://doi.org/10.1186/s41601-022-00244-z
16. Qu, S.; Xu, Y.; Huang, S.; Sun, M.; Wang, C.; Shang, Y. Recent Advancements in Optical Frequency-Domain Reflectometry: A Review. IEEE Sensors J. 2023, 23, 3949–3963. https://doi.org/10.1109/JSEN.2022.3227677

17. Hubbard, P.; Xu, J.Y.; Zhang, S.; DeJong, M.; Luo, L.; Soga, K.; Papa, C.; Zulberti, C.; Malara, D.; Fugazzotto, F.; et al. Dynamic structural health monitoring of a model wind turbine tower using distributed acoustic sensing (DAS). J. Civil Struct. Health Monit. 2021, 11, 833–849. https://doi.org/10.1007/s13349-021-00483-y
18. Amin, A.; Bibo, A.; Panyam, M.; Tallapragada, P. Vibration based fault diagnostics in a wind turbine planetary gearbox using machine learning. Wind Eng. 2022, 46, 1514–1526. https://doi.org/10.1177/0309524X221123968
19. Xu, J.T.; Luo, L.; Saw, J.; Wang, C.-C.; Sinha, S.K.; Wolfe, R.; Soga, K.; Wu, Y.; DeJong, M. Structural health monitoring of offshore wind turbines using distributed acoustic sensing (DAS). J. Civil Struct. Health Monit. 2024, 14, 805–824. https://doi.org/10.1007/s13349-024-00883-w
20. Teng, W.; Ding, X.; Cheng, H.; Han, C.; Liu, Y.; Mu, H. Compound faults diagnosis and analysis for a wind turbine gearbox via a novel vibration model and empirical wavelet transform. Renew. Energy 2019, 136, 393–402. https://doi.org/10.1016/j.renene.2018.12.094
21. Zhi, S.; Wu, H.; Shen, H.; Wang, T.; Fu, H. Entropy-Aided Meshing-Order Modulation Analysis for Wind Turbine Planetary Gear Weak Fault Detection under Variable Rotational Speed. Entropy 2024, 26, 409. https://doi.org/10.3390/e26050409
22. Abedin, S.; Biondi, A.M.; Wu, R.; Cao, L.; Wang, X. Structural Health Monitoring Using a New Type of Distributed Fiber Optic Smart Textiles in Combination with OFDR. Sensors 2023, 23, 1591. https://doi.org/10.3390/s23031591

